Supporting information

Stable acidic H_2O_2 electrosynthesis via *in situ* Ti-N bridging sites

Yuxiang Zhang [a], Shan Ding [a, b*], Sheng Chen [a*]

[a] Key Laboratory for Soft Chemistry and Functional Materials (Ministry of Education), School of Chemistry and Chemical Engineering, Nanjing University of Science and Technology, Ministry of Education, Nanjing, 210094, China

[b] Anhui Province Key Laboratory of Conservation and Utilization for Dabie Mountain Special Bio-Resources, West Anhui University, Lu'an, 237012, Anhui, China

*Corresponding e-mail: 18068841629@njust.edu.cn (S.D.); sheng.chen@njust.edu.cn

I. Experiment section

1. Synthesis of MIL-125

In a typical synthesis, H_2BDC (3.0 g, 18 mmol) was first dispersed in a mixed solvent of DMF and methanol (60 mL, 9:1 v/v) with stirring for 30 minutes. Following the dropwise addition of titanium isopropoxide (1.35 mL, 4.5 mmol), the mixture was stirred vigorously for 1 hour. The resulting solution was subjected to solvothermal treatment in a Teflon-lined autoclave at 160 °C for 20 hours. After cooling, the white product was collected, washed sequentially with DMF and methanol, and dried under vacuum at 60 °C for 12 hours.

2. Synthesis of MIL-125@ppy

To initiate polymerization, 20 mg of MIL-125 and 50 mg of sodium dodecyl sulfate were dispersed in 10 mL of water, followed by the addition of 0.1 mL of pyrrole. Subsequently, an aqueous solution of ammonium persulfate (500 mg in 10 mL) was combined with the dispersion, and the reaction proceeded at 0 °C for 12 hours. The resulting product was isolated, washed repeatedly with water, and dried at 60 °C to afford a black powder.

3. Physical characterizations

Morphological characterization was conducted using a ZEISS GeminiSEM 300 field emission scanning electron microscope. Transmission electron microscopy (TEM) and high-resolution TEM (HRTEM) were carried out on an FEI Talos F200X G2 instrument operated at 300 kV. X-ray diffraction (XRD) patterns were acquired on a Bruker D8 ADVANCE diffractometer equipped with Cu Kα radiation (λ = 1.5418 Å)

operating at 40 kV and 40 mA. X-ray photoelectron spectroscopy (XPS) measurements were performed on a Thermo Scientific K-Alpha spectrometer using an Al Kα source (1486.6 eV), with survey scans collected over a range of 0−1400 eV. Fourier transform infrared (FT-IR) spectra were recorded on a Thermo Scientific Nicolet iS5 spectrophotometer. Ultraviolet-visible (UV-vis) absorption spectra were obtained using a TU-1950 spectrophotometer. Electrochemical measurements were performed with a CHI660E electrochemical workstation connected with a high current amplifier in a standard three-electrode system. The ATR-SEIRAS spectra were recorded in a Bruker INVENIO FTIR Spectrometer.

4. Electrochemical tests in rotating ring-disk electrode system (RRDE)

Rotating ring-disk electrode (RRDE) measurements were performed with a glassy carbon disk and platinum ring in a three-electrode configuration. A catalyst ink was prepared by ultrasonicating 5 mg of catalyst and 40 μL of Nafion solution in 1 mL of a 3:1 (v/v) isopropanol/water mixture for 1 h. Then, 5 μL of the ink was drop-cast onto the disk electrode (geometric area: 0.2475 cm^2) to form a uniform film. The catalyst-coated disk electrode was used as the working electrode, with a carbon rod and a saturated Ag/AgCl electrode serving as the counter and reference electrodes, respectively. The ORR activity and H_2O_2 selectivity were assessed in O_2-saturated 0.5 M K_2SO_4 electrolyte (pH = 1) via linear sweep voltammetry (LSV) at a rotation rate of 1600 rpm. The ring potential was held at +1.2 V (*vs.* RHE) to oxidize H_2O_2 produced at the disk.

H_2O_2 selectivity and electron transfer number (n) were calculated from the disk (i_d) and ring (i_r) currents using the equations:

$$H_2O_2(\%) = \frac{2 \times \frac{i_r}{N}}{| i_d | + \frac{i_r}{N}} \times 100\%$$

$$n = \frac{4 \times | i_d |}{| i_d | + i_r/N}$$

Where i_d and i_r represent the disk and ring currents, respectively, and N is the RRDE collection efficiency, determined to be 0.37.

All of the LSV polarization curves are uncorrected for iR correction, and potentials are converted to the RHE scale via $E_{RHE} = E_{Ag/AgCl} + 0.059\ pH + 0.197$.

5. Electrochemical tests in flow-type electrolytic cell

The working electrode was prepared by dispersing 5 mg of catalyst and 50 μL of Nafion solution (5 wt%) in 950 μL of isopropanol, followed by ultrasonication for 1 h to form a homogeneous ink. The ink was spray-coated onto a gas diffusion layer (GDL) at a loading of 0.2 mg cm^{-2}. Electrochemical measurements were performed in a three-electrode flow cell using the catalyst-modified GDL as the working electrode, an IrO_2 electrode as the counter electrode, and an Ag/AgCl electrode (saturated KCl) as the reference. The cathode and anode compartments were separated by a Nafion 117 proton exchange membrane. During testing, the gas flow rate was maintained at 20 sccm.

The concentration of H_2O_2 in the catholyte was determined using a titanium sulfate ($Ti(SO_4)_2$) colorimetric method [1-3], which is based on the formation of a yellow peroxotitanium complex. The absorbance of the complex was measured at 408 nm by

UV-vis spectroscopy. A calibration curve was established using standard H_2O_2 solutions, and the concentration in experimental samples was determined by interpolating the measured absorbance into this curve.

The H_2O_2 yield rate (Y, mol g_{cat}^{-1} h^{-1}) and Faradaic efficiency (FE, %) were calculated using the following equations:

$$Y = \frac{c(H_2O_2) \times V}{\mathrm{M} \times \mathrm{t} \times s \times m_{cat}}$$

$$FE = \frac{2F \times c(H_2O_2) \times V}{34It}$$

Where $c(H_2O_2)$ is the concentration of H_2O_2 in cathode (mg L^{-1}), V is the volume of cathodic electrolyte (L), M (34 g mol^{-1}) is the relative molecular mass of H_2O_2, m_{cat} is the catalyst loading (mg cm^{-2}), s is the electrode area (cm^2), F is the Faraday constant (96485 C mol^{-1}), I is the applied current (A) and t is the electrolysis time (h).

II. Supplementary Results

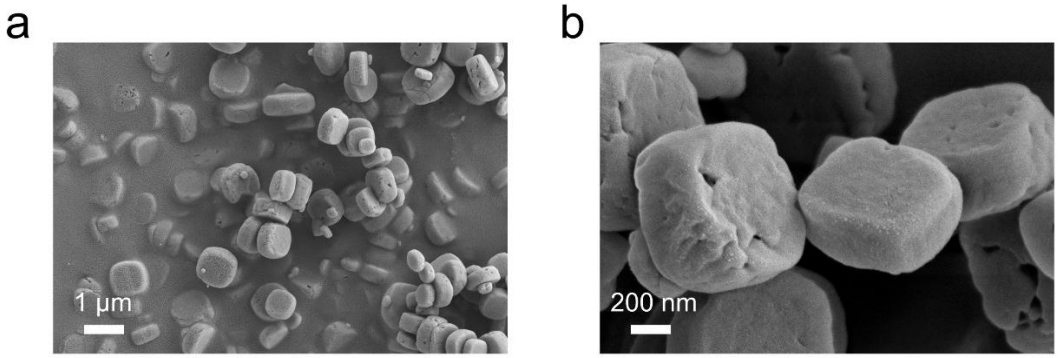

Figure S1 Scanning electron microscopy (SEM) image of MIL-125 (scale bar: 1 μm for a; 200 nm for b).

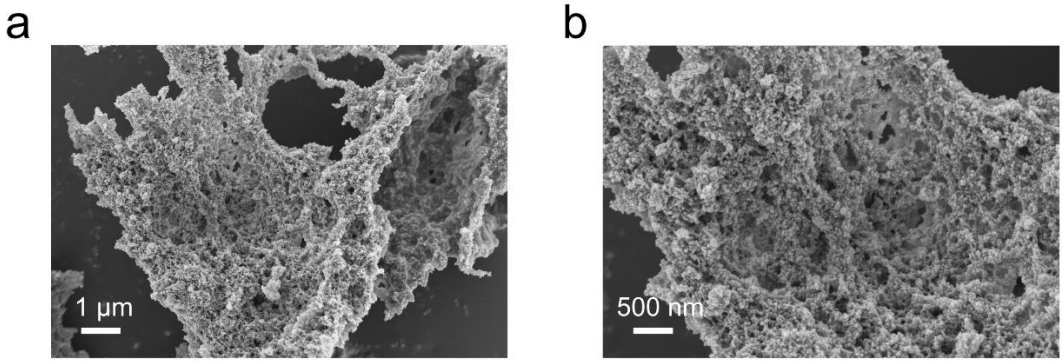

Figure S2 Scanning electron microscopy (SEM) image of Ppy (scale bar: 1 μm for a; 500 nm for b).

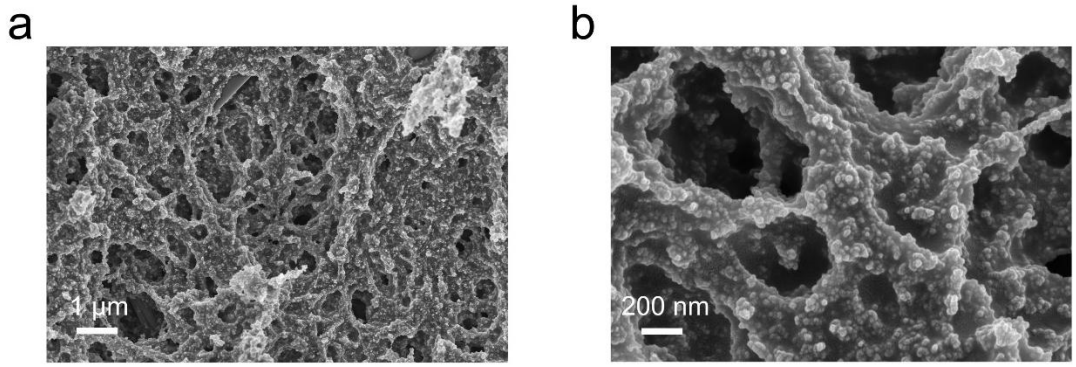

Figure S3 Scanning electron microscopy (SEM) image of MIL-125@Ppy (scale bar: 1 µm for a; 200 nm for b).

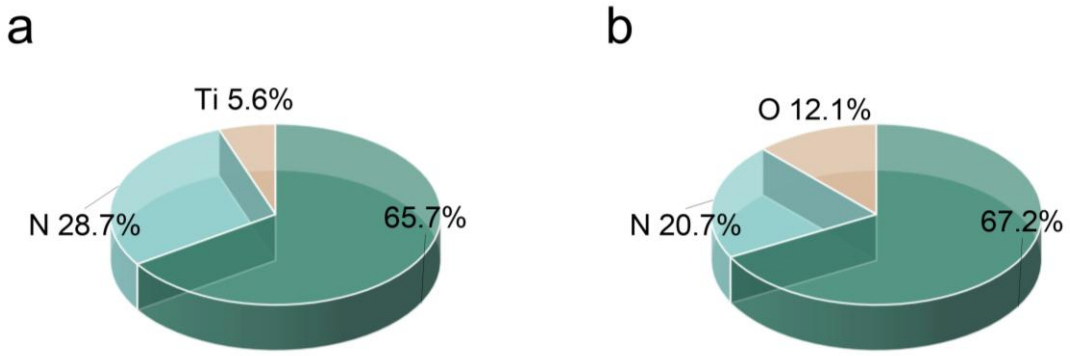

Figure S4 Charts showing the percentages of C, O, N and Ti elements by XPS results.

(a) MIL-125. (b) Ppy.

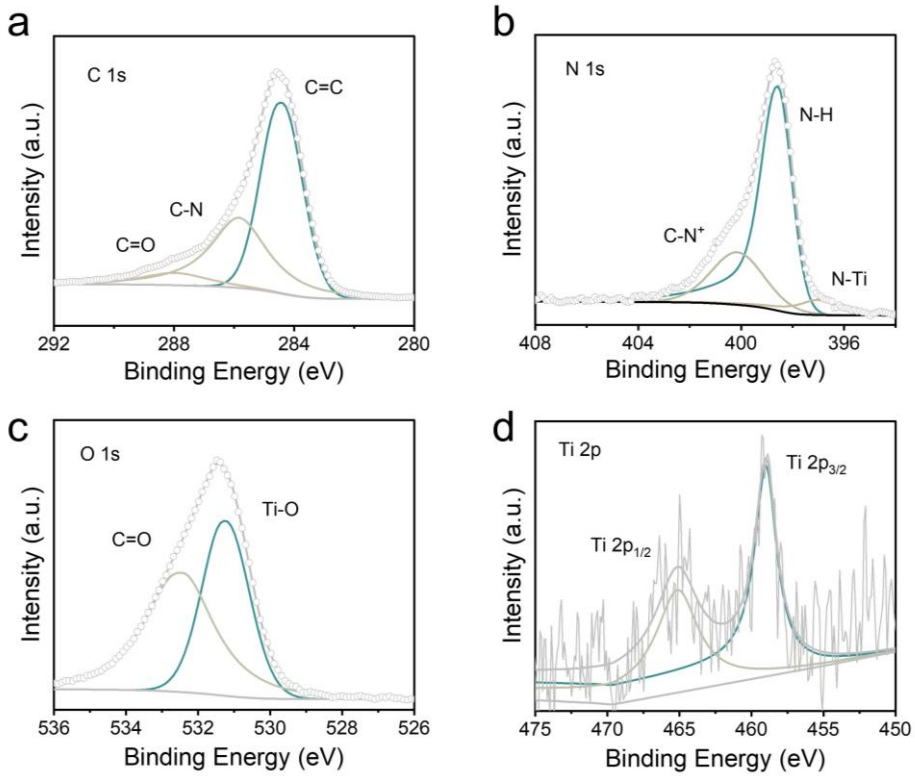

Figure S5 High-resolution XPS spectrums of MIL-125@Ppy. (a) C 1s. (b) N 1s. (c) O 1s. (d) Ti 2p.

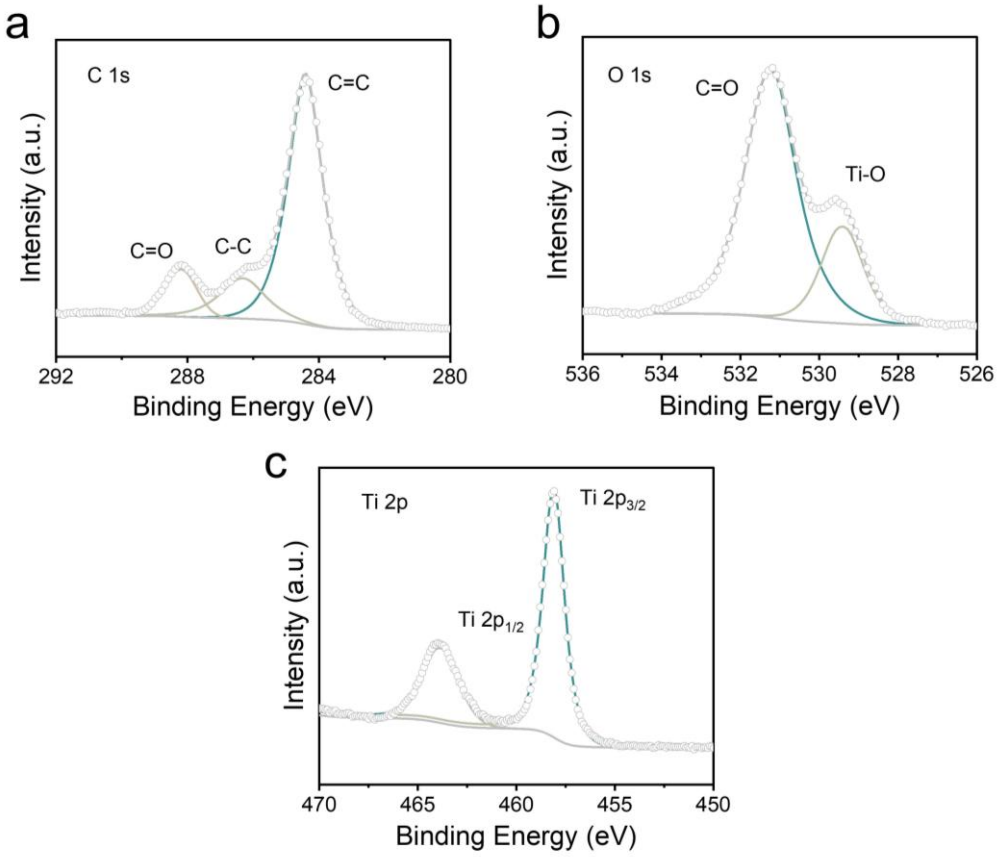

Figure S6 High-resolution XPS spectrums of MIL-125. (a) C 1s. (b) O 1s. (c) Ti 2p.

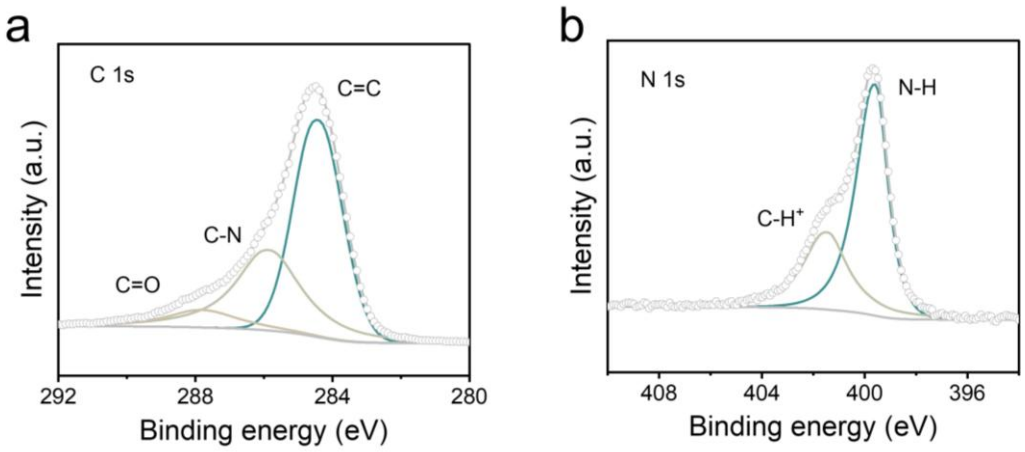

Figure S7 High-resolution XPS spectrums of Ppy. (a) C 1s. (b) N 1s.

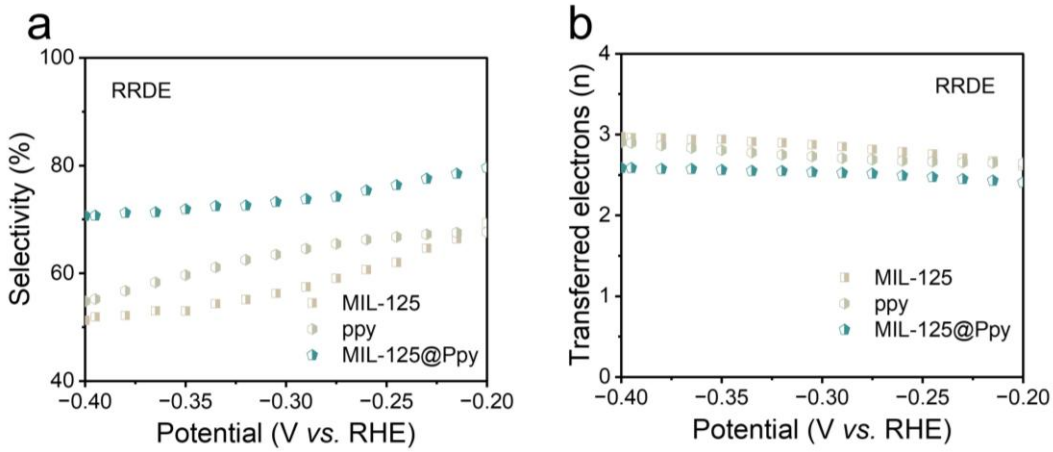

Figure S8 Calculated H_2O_2 selectivity (%) (a) and transferred electrons (n) (b) on MIL-125, Ppy and MIL-125@Ppy based on the RRDE measurements at pH = 1 under O_2 atmosphere.

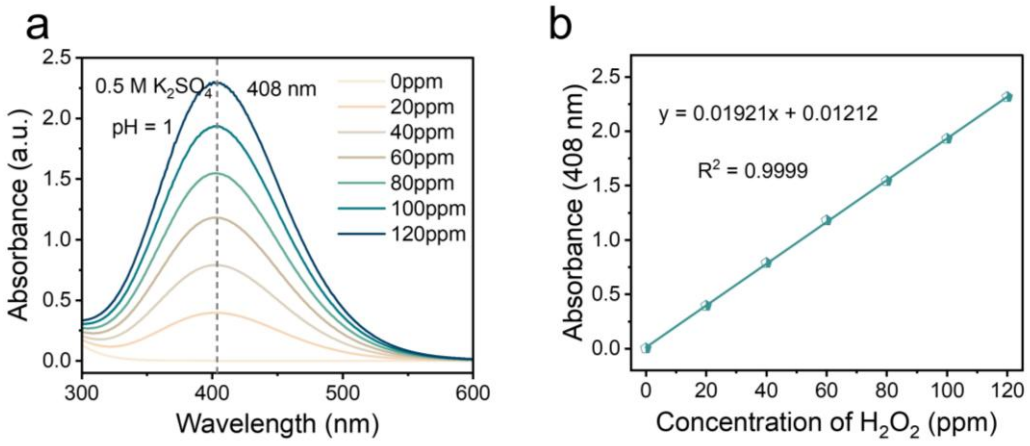

Figure S9 The calibration curve for hydrogen peroxide was measured by a traditional titration method in 0.5 M K_2SO_4 (pH = 1) electrolyte. (a) The standard UV-Vis adsorption spectra of H_2TiO_4 with different H_2O_2 concentrations; (b) Calibration curve used for estimation of H_2O_2 concentrations.

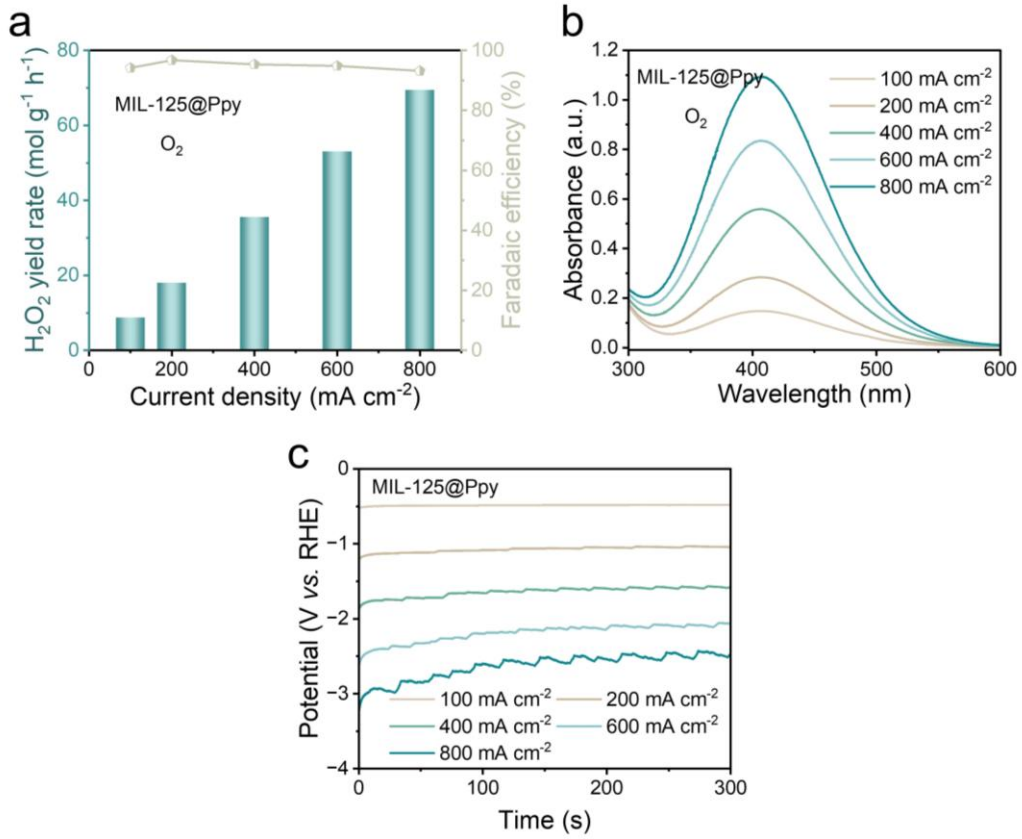

Figure S10 The $2e^-$ ORR performance of MIL-125@Ppy in flow cell (pH = 1, O_2). (a) The H_2O_2 yield rates and Faradaic efficiencies calculated by chronopotentiometry test; (b) The UV-vis spectra under chronopotentiometry test at different current densities. (c) The chronopotentiometry test of MIL-125@Ppy.

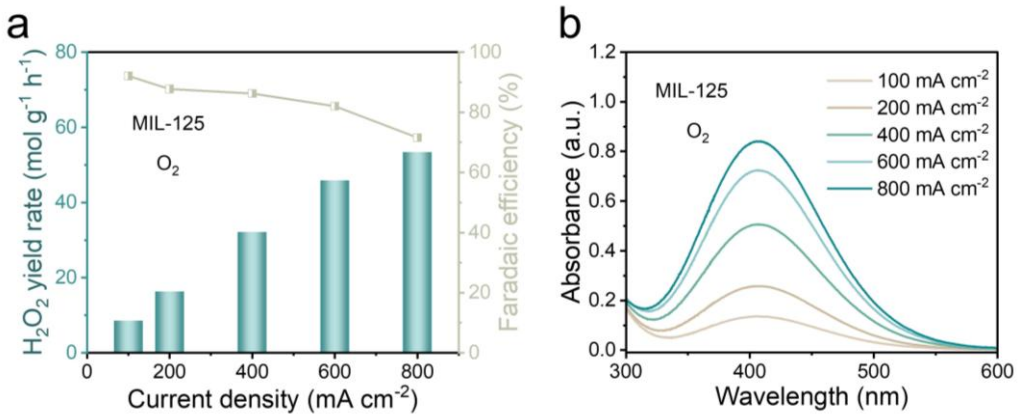

Figure S11 The $2e^-$ ORR performance of MIL-125 in flow cell (pH = 1, O_2). (a) The H_2O_2 yield rates and Faradaic efficiencies calculated by chronopotentiometry test; (b) The UV-vis spectra under chronopotentiometry test at different current densities.

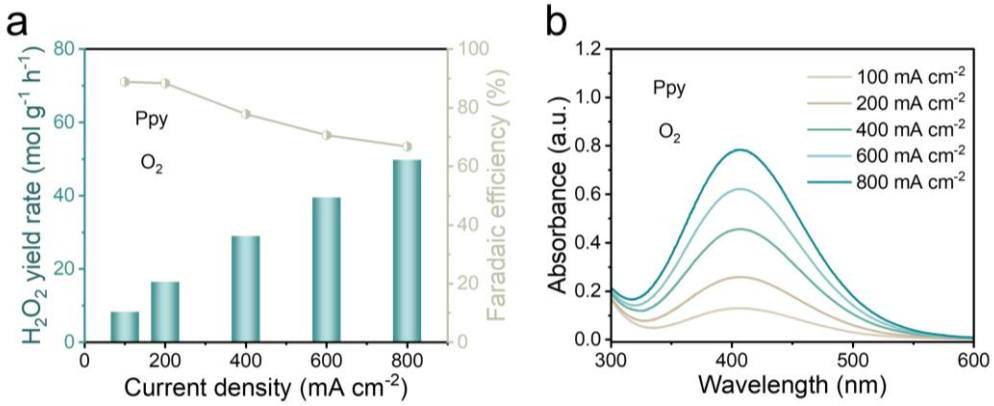

Figure S12 The $2e^-$ ORR performance of Ppy in flow cell (pH = 1, O_2). (a) The H_2O_2 yield rates and Faradaic efficiencies calculated by chronopotentiometry test; (b) The UV-vis spectra under chronopotentiometry test at different current densities.

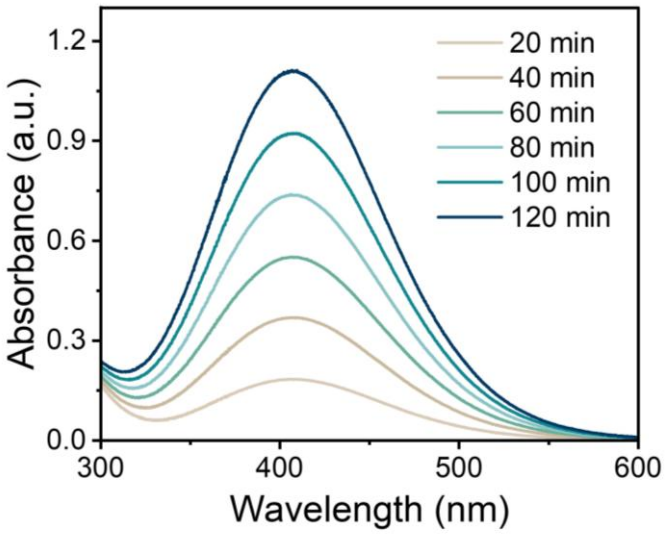

Figure S13 The corresponding UV-vis spectra of the cumulative H_2O_2 concentration of MIL-125@Ppy electrode in pH = 1.

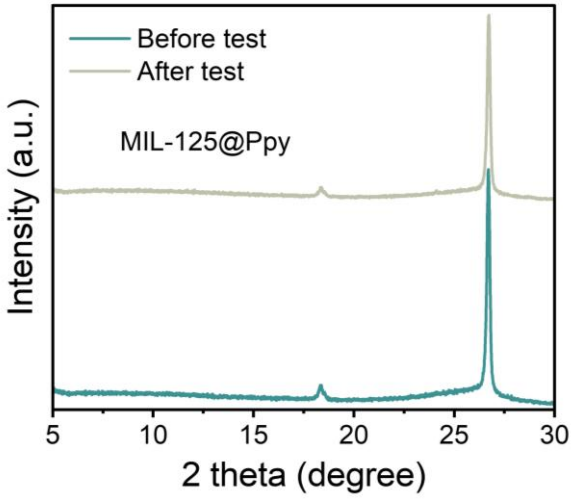

Figure S14 The XRD patterns of MIL-125@Ppy before and after the stability test.

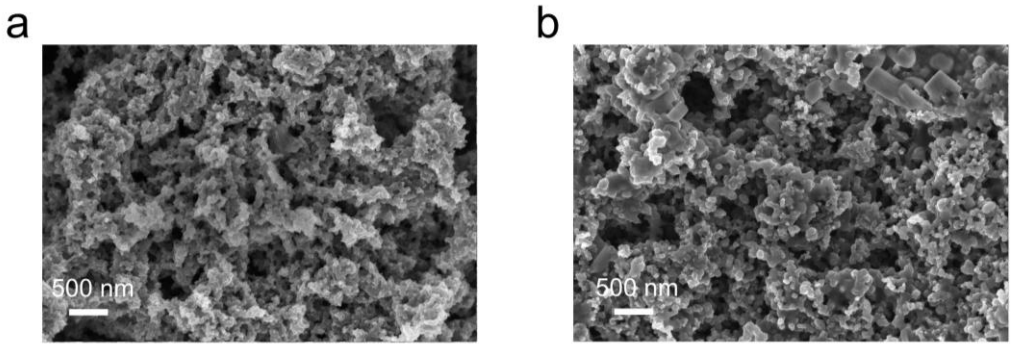

Figure S15 The SEM images of MIL-125@Ppy before and after the stability test. (a) Before test; (b) After test.

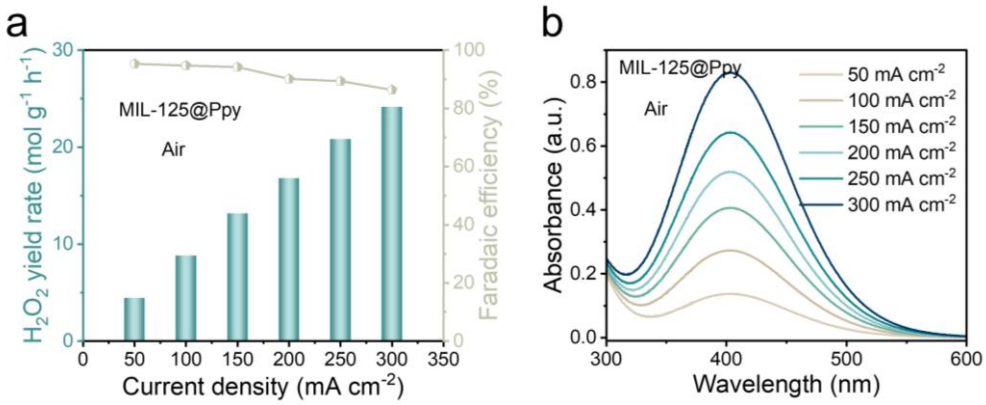

Figure S16 The $2e^-$ ORR performance of MIL-125@Ppy in flow cell (pH = 1, Air). (a) The H_2O_2 yield rates and Faradaic efficiencies calculated by chronopotentiometry test; (b) The UV-vis spectra under chronopotentiometry test at different current densities.

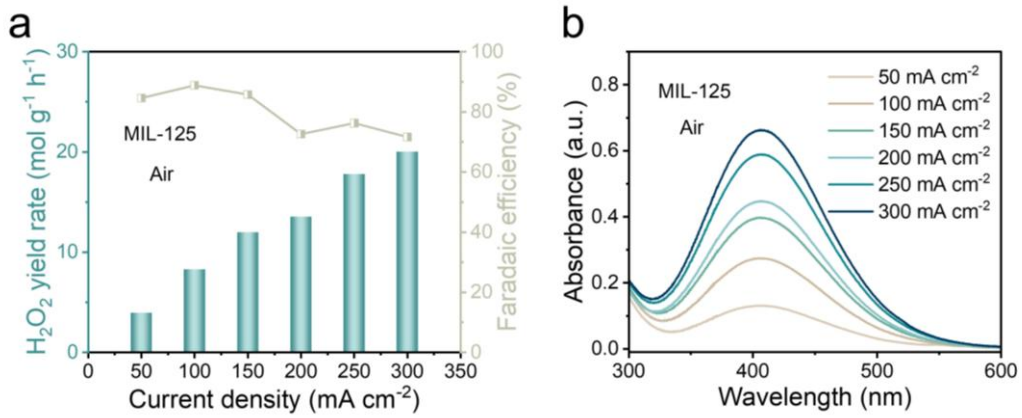

Figure S17 The $2e^-$ ORR performance of MIL-125 in flow cell (pH = 1, Air). (a) The H_2O_2 yield rates and Faradaic efficiencies calculated by chronopotentiometry test; (b) The UV-vis spectra under chronopotentiometry test at different current densities.

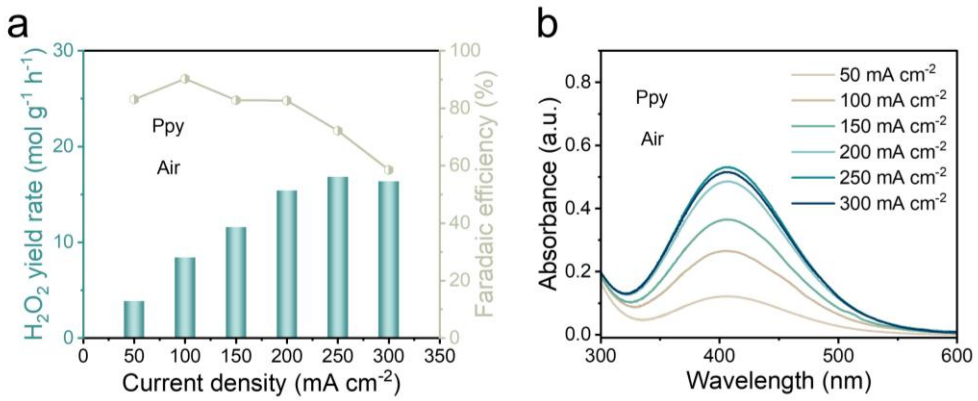

Figure S18 The $2e^-$ ORR performance of Ppy in flow cell (pH = 1, Air). (a) The H_2O_2 yield rates and Faradaic efficiencies calculated by chronopotentiometry test; (b) The UV-vis spectra under chronopotentiometry test at different current densities.

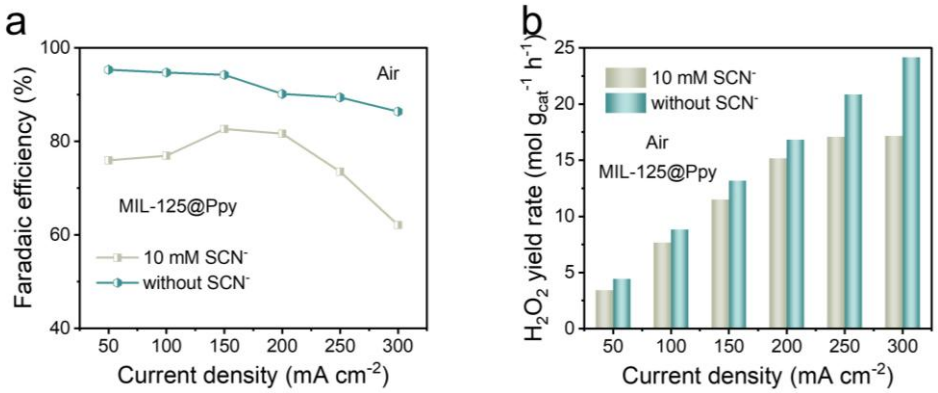

Figure S19 The comparison of $2e^-$ ORR performance with SCN^- toxicized and non-toxicized in flow cells. (a) H_2O_2 FEs; (b) H_2O_2 yield rates.

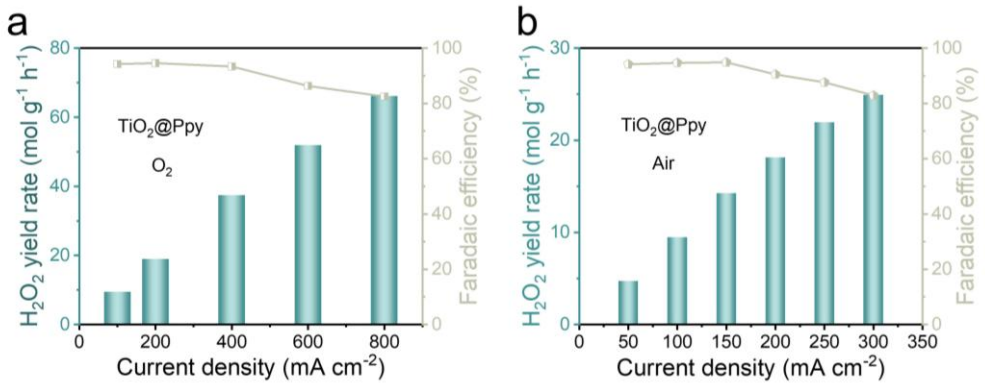

Figure S20 The $2e^-$ ORR performance of TiO_2@Ppy in flow cell (pH = 1). (a) O_2; (b) Air.

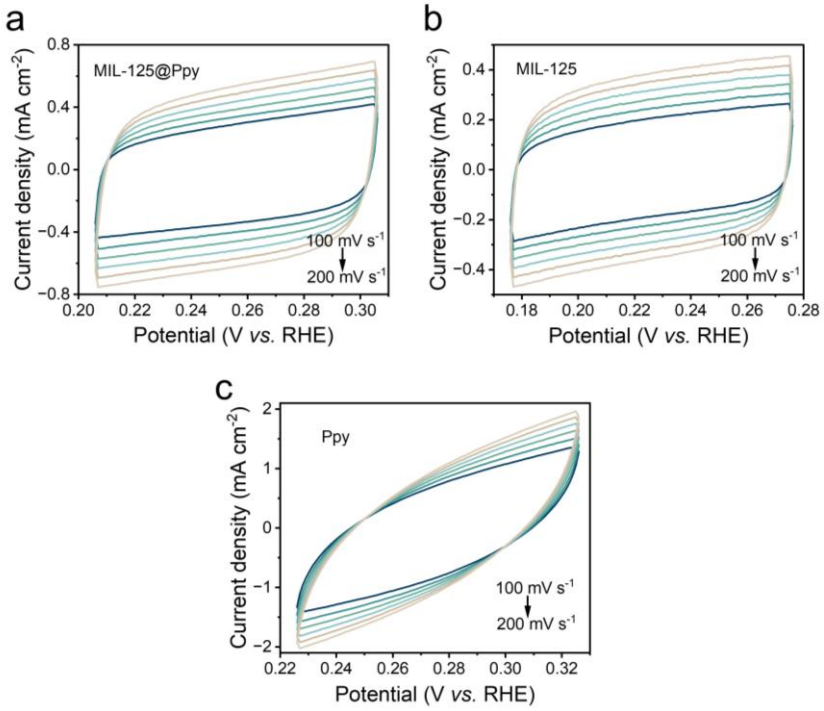

Figure S21 CVs measured at different scan rates from 100 to 200 mV s^{-1}. (a) MIL-125@Ppy, (b) MIL-125 and Ppy (c).

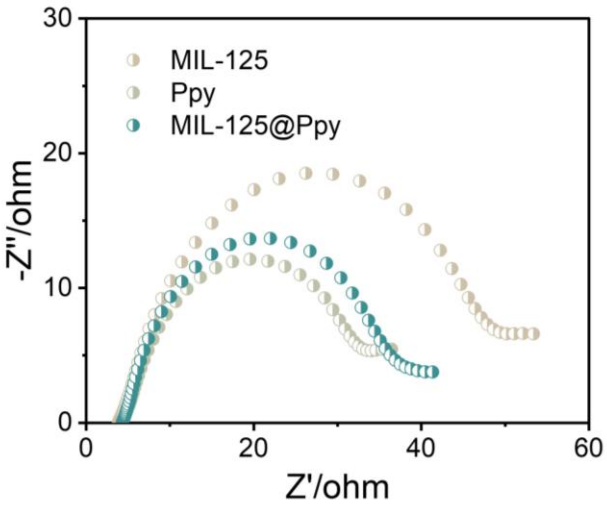

Figure S22 Electrochemical impedance spectroscopy (EIS) spectra of MIL-125@Ppy, MIL-125 and Ppy in 0.5 M K_2SO_4 (pH = 1) electrolyte.

Table S1 The comparison of Faradaic efficiencies (%) of MIL-125@Ppy with other counterpart under O_2 atmosphere in acidic electrolyte (pH = 1).

Current density (mA cm^{-2})	**MIL-125**	**Ppy**	**MIL-125@Ppy**
100	92.1	88.9	94.1
200	87.8	88.3	96.7
400	86.3	77.8	95.3
600	82.1	70.7	94.8
800	71.6	66.7	93.2

Table S2 The comparison of H_2O_2 yield rates (mol g_{cat}^{-1} h^{-1}) of MIL-125@Ppy with other counterpart under O_2 atmosphere in acidic electrolyte (pH = 1).

Current density (mA cm^{-2})	**MIL-125**	**Ppy**	**MIL-125@Ppy**
100	8.59	8.28	8.77
200	16.36	16.47	18.03
400	32.16	29.02	35.54
600	45.89	39.51	53.04
800	53.36	49.77	69.47

Table S3 The comparison of Faradaic efficiencies (%) of MIL-125@Ppy with other counterpart under air atmosphere in acidic electrolyte (pH = 1).

Current density ($mA\ cm^{-2}$)	**MIL-125**	**Ppy**	**MIL-125@Ppy**
50	84.6	83.1	95.3
100	88.8	90.3	94.7
150	85.8	82.8	94.2
200	72.6	82.7	90.2
250	76.3	72.2	89.4
300	71.6	58.5	86.4

Table S4 The comparison of H_2O_2 yield rates (mol g_{cat}^{-1} h^{-1}) of MIL-125@Ppy with other counterpart under air atmosphere in acidic electrolyte (pH = 1).

Current density (mA cm^{-2})	**MIL-125**	**Ppy**	**MIL-125@Ppy**
50	3.94	3.87	4.44
100	8.28	8.41	8.83
150	11.99	11.58	13.17
200	13.53	15.41	16.81
250	17.77	16.82	20.83
300	20.03	16.36	24.15

Table S5 The comparison of MIL-125@Ppy with state-of-the-art electrocatalysts towards $2e^-$ ORR in acidic electrolyte.

Catalyst	Atmosphere	Yield (mol g_{cat}^{-1} h^{-1})	Faradaic efficiency (%)	Current density (mA cm^{-2})	Reference
MIL-125@Ppy	O_2	69.47	93.2	800	This work
	Air	24.15	86.4	300	
Co_2-DAC [4]	O_2	11.72	85	400	J. Am. Chem. Soc. 2024, 146, 13, 9434–9443
Se_2-Pt NPs [5]	O_2	4.16	89.2	250	Nat. Commun. 15 (2024) 9346
Co_1/HCNF [6]	O_2	12.28	87	400	Adv. Mater. 2025, 37, 2418489
PD/N-C [7]	Air	5.34	89.0	50	J. Am. Chem. Soc. 145 (2023) 11589–11598
Co_1-NBC [8]	O_2	5.94	81.7	350	Angew. Chem. Int. Ed. 2025, 64, e202418713
CoIn-N-C [9]	O_2	9.68	80	100	Nat. Commun. 14

CoTPP@RGO-160 [10]	O_2	42.26	/	500	(2023) 4766 Angew. Chem. Int. Ed. 2024, 63, e202407163
Co-NC/MXenes [11]	Air	3.78	90.0	124.6	Appl. Catal. B Environ. Energy 317 (2022) 121737
CoPc/CNT [12]	Air	3.71	/	40	Chin. J. Catal. 43 (2022) 1238-1246
$Ni_3V_2O_8$-NS [13]	O_2	38.04	92.3	200	ACS Catal. 2024, 14, 16, 12140–12151

Supporting Reference

1. Q. r. Zhang, X. Tan, N. M. Bedford, et al., *Nat. Commun.*, 2020, **11**, 4181.
2. B. k. Xia, J. l. Du, M. Li, et al., *Adv. Mater.*, 2024, **36**, 2401641.
3. S. Ding, Y. x. Zhang, F. q. Lou, et al., *Mater. Today Energy*, 2023, **38**, 101430.
4. H. l. Huang, M. z. Sun, S. w. Li, et al., *J. Am. Chem. Soc.*, 2024, **146**, 9434−9443.
5. Z. y. Yu, H. Deng, Q. Yao, et al., *Nat. Commun.*, 2024, **15**, 9346.
6. J. Shim, J. Lee, H. Shin, et al., *Adv. Mater.*, 2025, **37**, 2418489.
7. C. Zhang, W. q. Shen, K. Guo, et al., *J. Am. Chem. Soc.*, 2023, **145**, 11589−11598.
8. S. y. Chen, T. Luo, J. y. Wang, et al., *Angew. Chem. Int. Ed.*, 2025, **64**, e202418713.
9. J. n. Du, G. k. Han, W. Zhang, et al., *Nat. Commun.*, 2023, **14**, 4766.
10. Y. h. Chen, C. Zhen, Y. b. Chen, et al., *Angew. Chem. Int. Ed.*, 2024, **63**, e202407163.
11. X. Huang, W. Zhang, W. Liu, et al., *Appl. Catal. B: Environ.*, 2022, **317**, 121737.
12. Z. x. Yu, C. Liu, Y. y. Deng, et al., *Chinese J. Catal.*, 2022, **43**, 1238−1246.
13. Z. k. Bao, W. j. Fang, J. y. Li, et al., *ACS Catal.*, 2024, **14**, 12140−12151.